Westward Intensification of the Mean Circulation on the Bering Sea Shelf*

THOMAS H. KINDER,** DAVID C. CHAPMAN AND JOHN A. WHITEHEAD, JR.

Woods Hole Oceanographic Institution, Woods Hole, MA 02543

(Manuscript received 1 August 1985, in final form 10 January 1986)

ABSTRACT

Most of the water that eventually flows northward through Bering Strait originates about 500 km south, seaward of the shelfbreak in the Bering Sea. Cumulative observational evidence supports the idea that most of this northward flow across the gently shoaling eastern Bering Sea continental shelf occurs as a western boundary current along the Siberian coast. A homogeneous rotating laboratory model and a barotropic numerical model each demonstrate this westward intensification of the mean flow. The intensification results from the well-known topographic β-effect: the combination of rotation and the depth decrease in the direction of flow acts in a similar fashion to the meridional gradient of the Coriolis parameter. For reasonable values of Bering Strait transport and shelf bottom friction, current speeds of 10–20 cm s^{-1} and a current width of ~50 km are predicted.

1. Introduction

The broad continental shelf of the Bering Sea is connected to the Arctic Ocean by Bering Strait (Fig. 1). A mean of 0.5–1.0 Sv (Sverdrup $\equiv 1 \times 10^6$ m^3 s^{-1}) flows northward through this strait, but only a few percent is supplied by river runoff (section 2). The origin and path of the cross shelf flow which supplies the Bering Strait outflow have not been established observationally and are presently a matter of conjecture. A synthesis of relevant observational evidence is offered (section 3) that supports the notion that the bulk of the transport which supplies the Bering Strait outflow occurs in the west, crossing the shelfbreak near Cape Navarin and flowing northward along the Siberian coast.

As a consequence, a significant mean cross-isobath flow must exist from the shelfbreak (~170 m depth) to the Strait (~50 m depth). Simple laboratory (section 4) and numerical (section 5) experiments demonstrate that the dynamical implications of drawing the Bering Strait outflow across a shoaling bottom on the rotating earth can explain the apparent westward intensification. The results are then interpreted in the context of the Bering Sea shelf circulation (section 6).

2. Oceanographic background

The geographical, hydrological, and hydrographical environment of the Bering Sea shelf constrains the possible sources for the Bering Strait outflow. The Bering Sea is about 40 percent abyssal plain exceeding 3500 m depth and about 40 percent continental shelf of less than 200 m depth (Fig. 1). The eastern continental shelfbreak, which occurs at a mean depth of slightly less than 200 m, extends about 1000 km from Unimak Pass in the southeast to Cape Navarin in the northwest. The shelf is bounded by land on three sides: the Alaska Peninsula in the southeast, the Alaska mainland in the northeast, and Siberia in the northwest. Isobaths generally tend northwest–southeast, parallel to the shelfbreak. From the shelfbreak to the Alaska mainland is a distance of about 500 km, so the eastern Bering Sea shelf is one of the widest (and flattest) shelves in the world ocean. Bering Strait is a narrow (85 km) and shallow (50 m) connection between the Bering Sea shelf and the Chukchi Sea (and thence the Arctic Ocean) farther north. St. Lawrence Island bifurcates the southern approaches to the Strait, although there are passages on both the western and eastern sides of the island (sometimes called Anadyr and Shpanberg Straits, respectively).

Large volumes of freshwater are discharged onto the shelf, notably from the Yukon, Kuskokwim, and Anadyr Rivers. Estimates of the mean annual runoff are in the range of 8.0–10.0 $\times$ 10^3 m^3 s^{-1} (Roden, 1967; Coachman, Aagaard, and Tripp, 1975). This freshwater discharge has a large seasonal variation, with a minimum in spring and maximum in early summer (Ingraham, 1981; Overland, 1981). Runoff is roughly in phase with the Bering Strait transport, but, as discussed in the next section, it is not thought to cause the transport fluctuations.

There have been several systems proposed for classifying the waters of the shelf in terms of temperature, salinity or stratification (e.g., Ohtani, 1973; Coachman

* Woods Hole Oceanographic Institution Contribution Number 5994 and Naval Ocean Research and Development Activity Contribution Number 330:052:85.

** Permanent affiliation: Naval Ocean Research and Development Activity, NSTL, MS 39529.

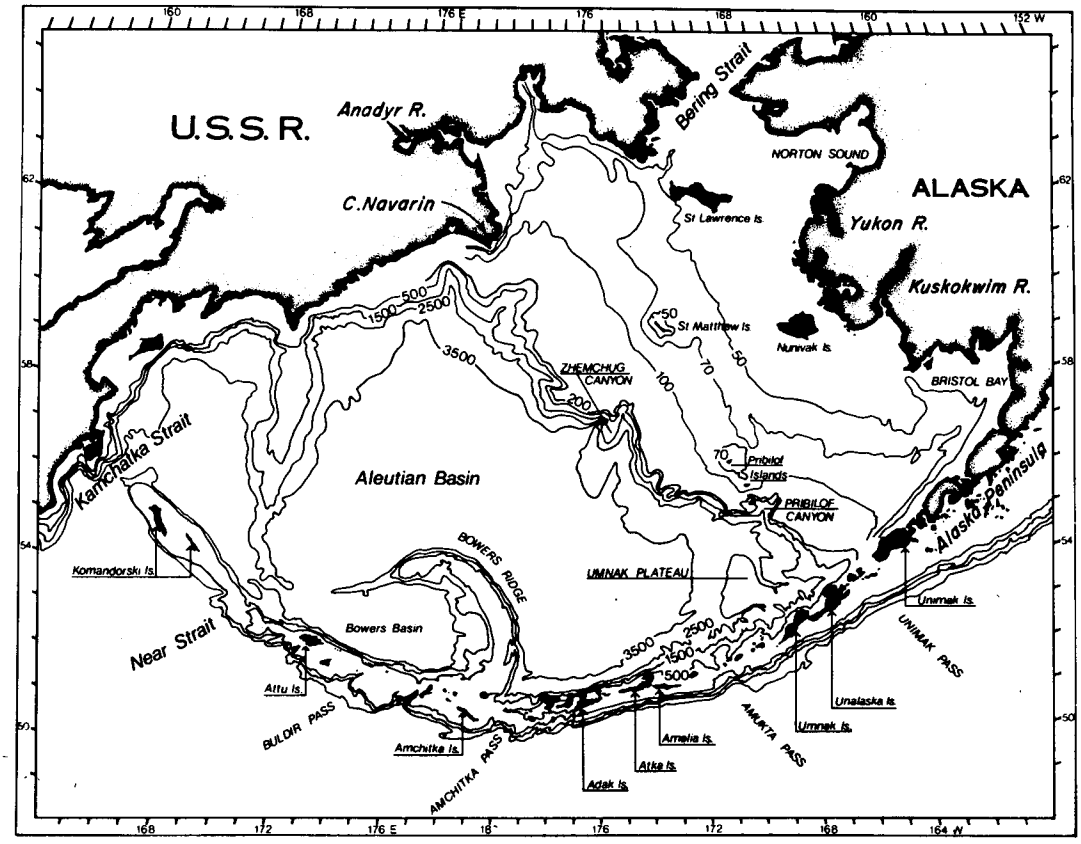

FIG. 1. The Bering Sea (depths in meters). (Figure courtesy of T. Paluszkiewicz.)

et al., 1975; Kinder and Schumacher, 1981a; Ingraham, 1981). It is most revealing for our purposes to focus attention on the salinity distribution. There is a basically monotonic decrease of salinity (surface, bottom, or depth-averaged) from the shelfbreak to the Alaska mainland (Ohtani, 1973; Ingraham, 1981). For instance, long-term mean July salinities (expressed in nondimensional units equivalent to parts per thousand) range from 33 at the 200 m isobath to 31 near the Alaska coast. This pattern can be temporarily upset during winter in regions where freezing occurs repeatedly because of the brine drainage from the ice (e.g., Schumacher et al., 1983), but otherwise the pattern persists throughout the year. Figure 2 shows the summer (June–September) distribution pattern for the years 1962–64 (Ohtani, 1973). A significant feature of this distribution is the high salinity tongue that extends from the deep basin near Cape Navarin through the Gulf of Anadyr to Bering Strait. The implication is that there is a considerable flow of water across the shelfbreak toward the Strait.

In the Strait itself, higher salinity water (known as "Anadyr water") is found on the Siberian side in both synoptic surveys and in mean composites (Fig. 3). Coachman et al. (1975) distinguish three water masses based on salinity. In 1967, for example, they reported

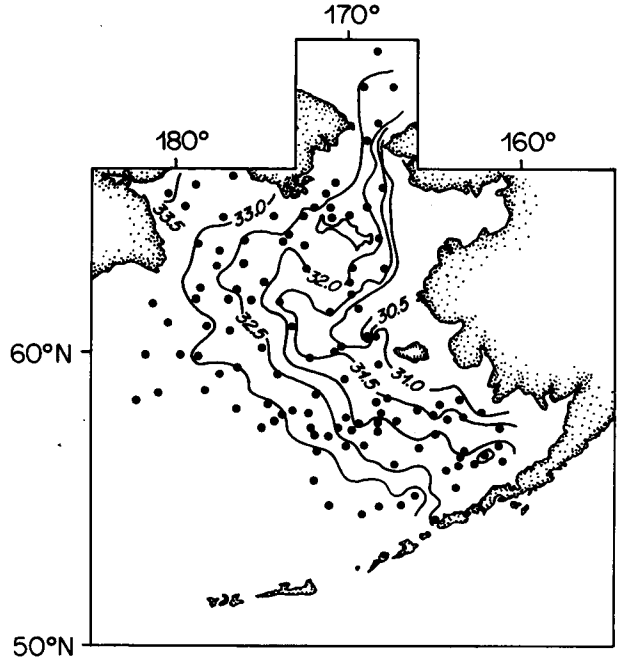

FIG. 2. Salinity distribution at the bottom of the shelf in summer, based on *Oshoro Maru* data from 1962–64. Note the tongue of higher salinity along the Siberian coast (from Ohtani, 1973).

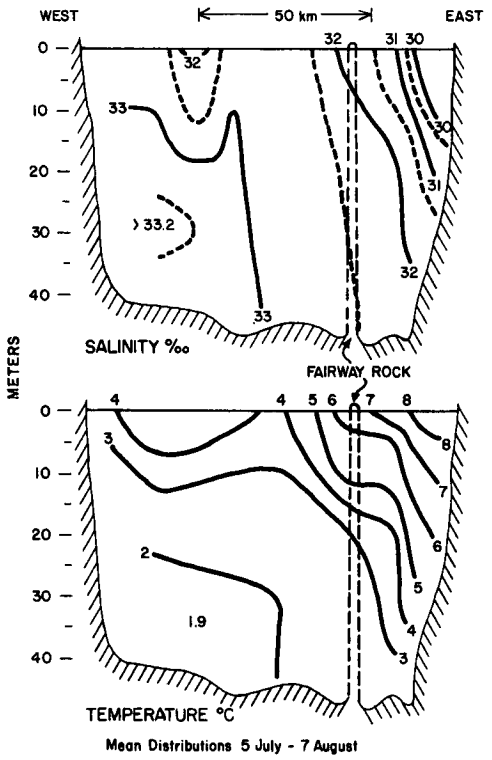

FIG. 3. Mean salinity and temperature distribution for Bering Strait for early summer. Water that is relatively warm and low in salinity is found on the Alaska side, and cooler, higher salinity water is found on the Siberia side (from Coachman et al., 1975). (Copyrighted figure courtesy of University of Washington Press, Seattle.)

median salinities of 33 for Anadyr water, 32.5 for "Bering Shelf" water, and 31.5 for "Alaskan coastal" water for sections across the Strait. Anadyr water is also higher in nutrients, a characteristic of the water overlying the deep basin and not over the shelf in general (Sambrotto et al., 1984). There are also large concentrations of oceanic copepods found near St. Lawrence Island whose likely source is advection from seaward of the 100 m isobath (Springer and Roseneau, 1985).

3. Bering Strait outflow and its source

Available direct current measurements are inadequate to estimate the transports and to infer the locations of the significant mean currents across the entire shelf. Adequate measurements exist in the Bering Strait region and over the southeastern shelf, and also probably along the continental slope. By using estimates of river runoff and salinity as a water mass tracer to supplement these measurements, a useful synthesis of the shelf water balance can be constructed.

In the Bering Strait the mean flow is probably driven by the Pacific sea level which stands higher than the Atlantic, but atmospheric forcing causes large fluctuations on many time scales (Coachman et al., 1975; Stigebrandt, 1984; Aagaard et al., 1985). Sections of velocity across the Strait (Fig. 4) typically show a high speed jet coincident with the low salinity coastal water on the Alaskan side, but there is also a considerable northward flow of the higher salinity Anadyr water on the Siberian side. Data near the Siberian side of the Strait are sparse because of diplomatic difficulties. The Bering Strait flow has an annual cycle, with a July maximum $\sim$ 0.7 Sv and a February minimum $\sim$ 0.4 Sv (Coachman and Aagaard, 1981; Aagaard et al., 1985). The mean is about 0.6 Sv (Coachman et al., 1975; Coachman and Aagaard, 1981; Aagaard et al., 1985).

River runoff only accounts for a few percent of the Bering Strait outflow, so that the remainder of the water to supply this flow must come ultimately from off the shelf, over the slope or the deep basin. Numerous paths have been proposed for this flow, many of them apparently based on intuition in the absence of adequate data. Hughes et al. (1974) presented six examples that span a wide range of circulation patterns. Recent ideas, based on improved hydrographic measurements and some direct current measurements, have converged so

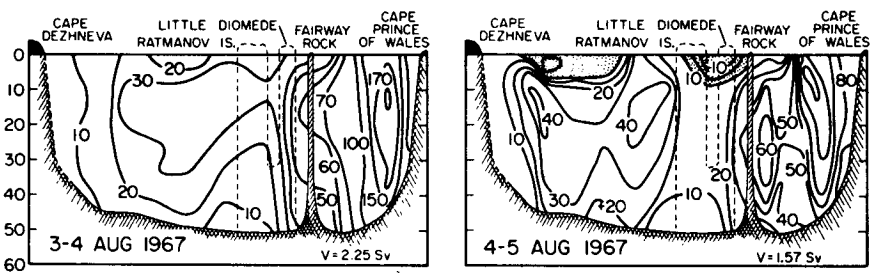

FIG. 4. Velocity (cm s^{-1}) obtained by lowering a current meter from an anchored ship during August 1967. Shaded areas represent southward flow. Estimated transports were 2.2 and 1.6 Sv (1 Sv $\equiv$ 1 $\times$ 10^6 m^3 s^{-1}) northward (from Coachman et al., 1975). These synoptic transport measurements are much higher than the maximum mean monthly transport. The hypothesized western boundary current probably supplies the northward flow of higher salinity water in the western two-thirds of the Strait. (Copyrighted figure courtesy of University of Washington Press, Seattle.)

that two paths to the Strait are likely: a buoyancy (low salinity) current beginning along the Alaska Peninsula and following the Alaskan coast northward, and a saline western boundary current, beginning at Cape Navarin and flowing northward along the Siberian coast (e.g., Takenouti and Ohtani, 1974).

In the south, the eastern current appears to be weak (a few cm s^{-1}) but persistent throughout the year. Kinder and Schumacher (1981b) used long-term current measurements to estimate a mean transport of 0.08 Sv near Nunivak Island. Thus, this flow plus river runoff accounts for only 15 percent of the Bering Strait outflow, and roughly corresponds to the low salinity Alaskan coastal water found on the Alaskan side of the Strait (Coachman et al., 1975).

Other than the Unimak Pass region near the Alaska Peninsula, there is no direct or indirect evidence of net cross-shelfbreak flow south of Cape Navarin. Extensive current and hydrographic measurements over the southeastern shelf during the past decade have shown no net onshelf or offshelf flow between Unimak Pass and the Pribilof Islands (Schumacher and Kinder, 1983; Coachman, 1986). Hydrographic, drifter, and satellite infrared studies along the slope show that the northwestward flowing Bering Slope Current carries up to 5 Sv, but it appears to parallel the slope until Cape Navarin (Kinder et al., 1975; Kinder et al., 1980; Paluskiewicz and Niebauer, 1984; Royer and Emery, 1984). Recent wintertime current and hydrographic measurements on the shelf northwest of the Pribilofs likewise show flow that is predominantly along the isobaths (Muench and Schumacher, 1985).

Over much of the shelf between the 100 and 50 m isobaths there exists a cold bottom layer that persists throughout the summer (Ingraham, 1981; Coachman, 1986). This cold water is formed annually by convection, and is isolated from the shallow layer by stratification that results from melting ice and insolation (Kinder and Schumacher, 1981b; Coachman, 1986). This layer forms a distinct temperature minimum across the middle shelf that could not persist in the face of significant northward advection (that is, a large component of flow normal to the isotherms).

In summary, there are no current measurements close to the Siberian coast known to us, but there is a strong salinity signal there. This evidence combined with the lack of evidence for flow of sufficient quantity elsewhere, suggests that the most likely location of the remaining 85 percent of the outflow supply is along the Siberian coast, in a western boundary current, more or less coincident with the salinity tongue. Figure 5 schematically illustrates the Bering Slope Current and the two currents leading from the deep basin to Bering Strait. Some of the water must undergo significant modification through mixing with the less saline shelf water before it reaches the Strait, because the high salinity Anadyr water apparently does not contribute 85 percent to the outflow transport in the Strait (Figs. 3 and 4). In the Strait, the western boundary current contribution probably corresponds to the Anadyr and Bering Shelf waters. A western boundary current thus seems likely, although confirmation by direct measurement is absent from the literature. In the following two sections the physics of such a current is examined using simple laboratory and numerical experiments.

4. Laboratory model

Several laboratory observations of western intensified currents have been made to study the general ocean circulation. For example, Beardsley (1969) and Baker and Robinson (1969) simulated the β-effect (the meridional gradient of the Coriolis frequency) using bottom topography—depth was varied linearly so that the deep end of the tank corresponded to the south, the shallow end to the north, and the right- and left-hand sidewalls (looking from deep to shallow) corresponded to east and west boundaries, respectively. In both experiments the sidewalls were circular, so that the precise definition of the eastern and western walls was unclear. Forcing was produced by a rotating lid which served as a distributed source and sink to the interior flow through the agency of Ekman suction. This forcing was meant to be a model of wind acting on the surface of the ocean and not just a local sink. In another type of experiment Stommel et al. (1958) and Kuo and Veronis (1971) used a local source, but a distributed sink: water level was allowed to rise during their experiments. The beta effect was simulated by the parabolic slope of the water surface, although Kuo and Veronis (1971) also varied the bottom to study topographic–rotational effects.

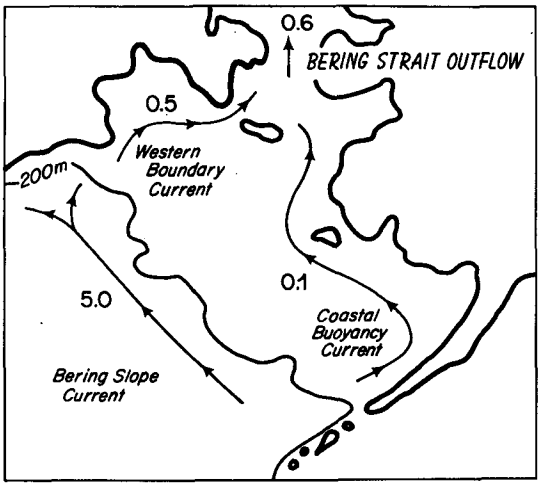

FIG. 5. Schematic of currents that supply the Bering Strait outflow. The numbers are transport in Sv (1×10^6 m^3 s^{-1}), and are intended to suggest relative sizes of the flows only. Two currents supply the outflow: a coastal buoyancy current along the Alaska coast and a western boundary current along the Siberia coast.

This concept of a western-intensified, source–sink flow was applied to the Bering Sea Shelf by placing a local sink near the center of a coast. In the (topographic) beta plane analogy, the sink is in the center of the zonal northern coast. To accomplish this a plywood false bottom with a slope of 1:5 was placed in the two meter turntable at the Coastal Research Center of the Woods Hole Oceanographic Institution (Fig. 6). The tank was filled with 23 cm of thymol-blue water solution and rotated at a period of 15 s so that the test fluid experienced a topographic β-effect (see section 5 for further discussion on topographic beta). The bottom was painted white and a square grid of lines painted so that the grid spacing was 10 cm in both directions when viewed directly from above. False walls were placed at each of the sloping ends of the false bottom and also at the deep end. These walls corresponded to the eastern, southern and western walls of a topographic beta plane. Electrode wires for flow visualization were mounted 22 cm above the true bottom of the tank. They were spaced parallel to the western wall at distances of 10, 50, 90, 120 and 160 cm, and parallel to the northern shoreline at distances of 10, 30, 50, 72 and 83 cm. The tank was carefully covered with transparent plastic during each run so that there was little or no wind stress on the water due to the rotation of the tank. A moveable sink, consisting of an oval pipe connected by hose to a pump, was placed at the northern shoreline of the test fluid at various distances from the western wall (Fig. 6). A run commenced after the fluid was spun up. The pump (sink) was then started and the evolution of the dye recorded by a 35-mm camera above the tank.

Figures 7–9 show selected photographs of the ensuing dye lines. In run 1 (Fig. 7), the sink was in the middle of the shelf, and it is obvious that the current flowed up the western wall and along the shallow part of the shelf to the sink. There was little or no current elsewhere, neither to the right of the sink nor in the interior of the fluid. Figures 8 and 9 show results from runs in which the sink was located on the left (western) side and the right (eastern) side of the coast, respectively. The results were the same in that most of the water moving up the shelf did so in the western boundary current. The lack of currents elsewhere was indisputable. Moreover, the pumping rates of the sink were different, but the thickness of the western boundary current seemed unaffected.

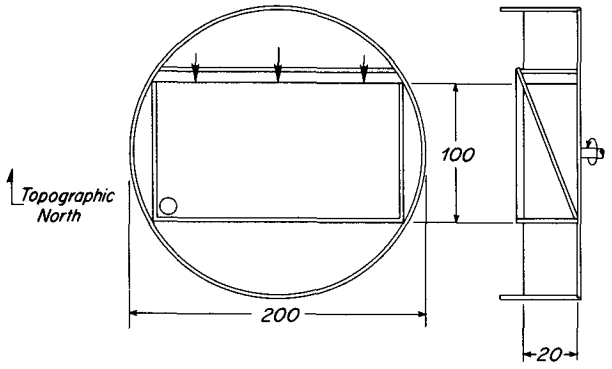

FIG. 6. Diagram of laboratory apparatus. Top view is on the left and a side view (with the vertical exaggerated by 2) is shown on the right. The arrows show individual locations of the sink and the circle in the lower left corner is the gravity return flow through a hole in the false bottom.

There are two classical length scales for the width of the western boundary current in this experiment if the flow is linear. One is due to bottom friction (Stommel, 1948) while the other is due to lateral friction of the interior fluid (Munk, 1950). The Stommel scale may be estimated by

$$W_s = (\nu/2f\tan^2\alpha)^{1/2}$$

where f is the Coriolis parameter, ν the kinematic viscosity of the fluid, and $\tan\alpha$ the bottom slope (from Pedlosky, 1979; pp. 177, 264 with $\beta_0 = f\tan\alpha/d$ where d is the depth of the fluid). The Munk scale is

$$W_m = 2\pi(\nu/\beta)^{1/3}3^{-1/2} = 2\pi(\nu d/f\tan\alpha)^{1/3}3^{-1/2}$$

(Pedlosky, 1979, p. 262). Using $d = 10$ cm, $f = 4\pi/15$ s^{-1}, $\tan\alpha = 0.2$ $\nu = 0.01$ cm^2 s^{-1}, $W_s = 0.4$ cm and $W_m = 3.1$ cm. The observed width of the western boundary current, at a water depth of 10 cm (about the third dye line from the top), is $\sim$10 cm in Fig. 7, $\sim$7–8 cm in Fig. 8, and probably close to 15 cm in Fig. 9. The Munk scale appears to be more consistent with the observations, but the observed widths are significantly larger than either of the linear predictions.

Another possible length scale for the width of the western boundary current is that of an inertial boundary layer in which nonlinear advection dominates. The degree of nonlinearity in the present experiments can be estimated by comparing the bottom friction time scale, $T_F = d(2/\nu f)^{1/2}$, to the advective time scale, $T_A = L/U$, where L is the shelf width and U is a typical velocity in the boundary layer. From Figs. 7–9, $U \approx 0.5$ cm s^{-1}, so $T_F/T_A \approx 0.77$ suggesting that the advective effects are of the same order as the bottom friction effects. Thus, an inertial boundary layer appears possible.

The steady-state width of an inertial boundary current is estimated by

$$W_I = (-V_I d/f\tan\alpha)^{1/2}$$

where V_I is the interior velocity normal to the boundary layer which is necessary to balance the "eastward" propagating topographic Rossby waves (Pedlosky, 1979, p. 280). For an inertial boundary layer of width $W_I = 10$ cm, an interior velocity of $V_I = -1.7$ cm s^{-1} is required. However, the large westward displacements of the north–south dye lines implied by this interior velocity were not observed in Figs. 7–9. Therefore, either the inertial scale does not apply here or the ex-

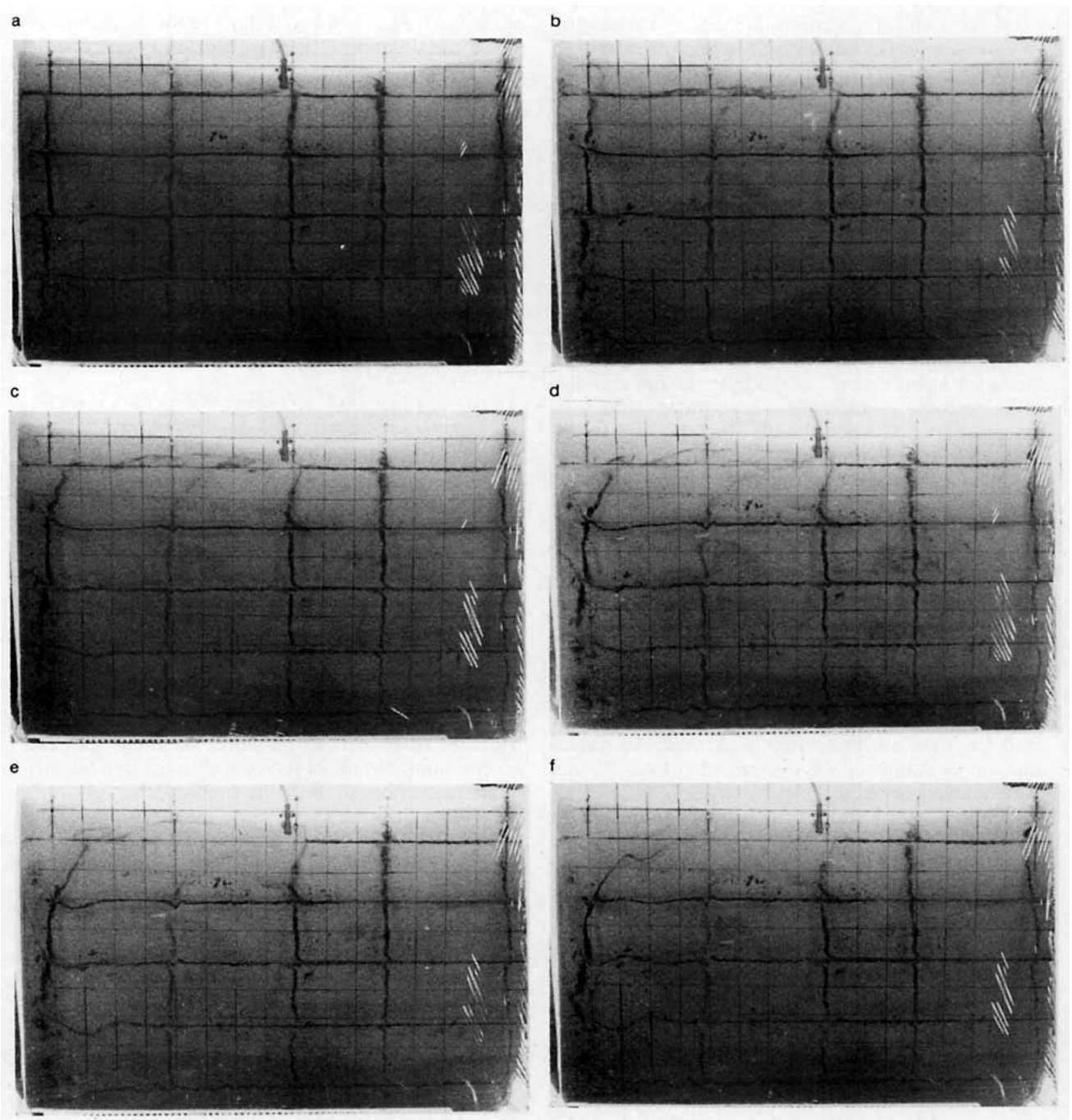

FIG. 7. Top view of the evolution of a rectangular grid of dye in a rotating fluid with a sloping bottom. A sink is located at the center of the coast (top), east is to the right and west is to the left. The dye has been in place for at least 60 seconds before the first photograph was taken. The grid painted on the bottom has a spacing of 10 cm. Times after start of the sink are 10, 20, 30, 40, 50 and 120 seconds for *a* through *f*, respectively. Period of rotation is 15.05 seconds and volume flux of the sink is 24 $cm^3\ s^{-1}$. The principal currents are eastward along the coast toward the sink, and northward along the western boundary. Note the absence of a current in the interior of the shelf and in the region east of the sink. The randomly positioned dark spots between dye lines are bits of a floc near the bottom of the tank, and should be disregarded.

perimental western boundary current has not reached steady state.

The volume flux of the western boundary current has been estimated from the photographs corresponding to 20, 30 and 40 seconds in Fig. 7. At 20 seconds, the third horizontal line from the top of the photograph (at 10 cm depth) has just begun to move. The areas that the dye line has traversed at 30 and 40 seconds

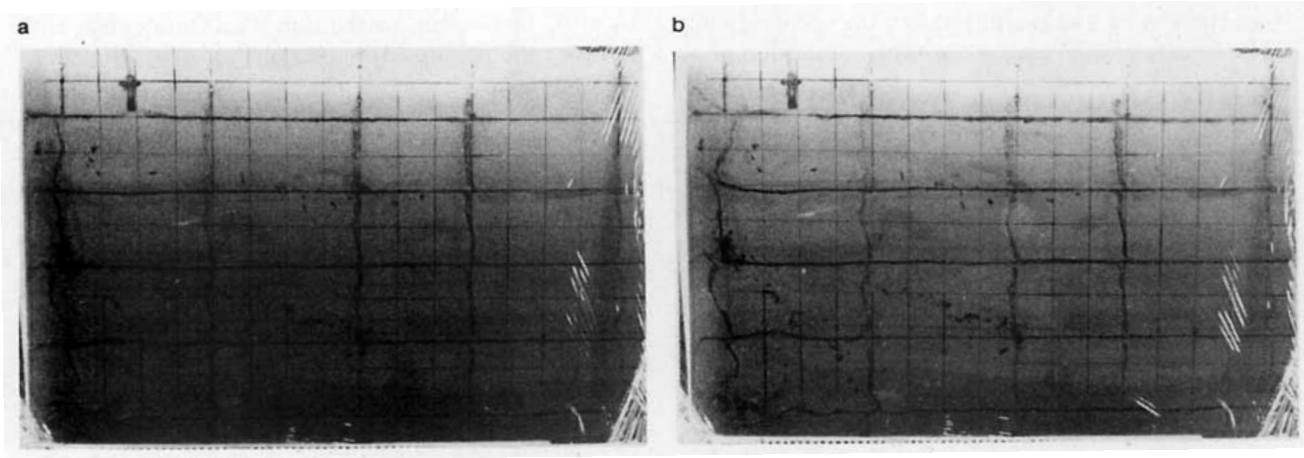

FIG. 8. The same type of experiment as in Fig. 7 except the sink is near the west coast. The northward current along the western boundary is clear and there is no detectable current in the interior and east of the sink. Times after start of the sink are 5 and 25 seconds. Period of rotation is 15.5 s and volume flux is 16 $cm^3 s^{-1}$.

were approximated as triangles with a base of 10 cm and heights of 5 cm and 10 cm, respectively. These correspond to volume displacements of 250 cm^3 and 500 cm^3, respectively. The measured volume flux of the pump was 24 $cm^3 s^{-1}$, which displaces 240 cm^3 in 10 s. Thus, to the accuracy of the experimental measurements (~10%), the western boundary current is observed to contain the volume flux of the pump, and the current carries all the water on the shelf that goes into the sink.

We conclude that the laboratory experiment demonstrated a western boundary current with a width somewhat greater than that expected by frictional theory. The boundary current may be inertial in which case it must still be evolving in time. The important point is that all of the flow into the sink came via the western boundary current, and none was detected elsewhere.

5. Numerical model

In this section, a numerical model is used to investigate both the dynamics of the laboratory experiment described in section 4 and the dynamics of the Bering Sea circulation described in sections 2 and 3. Since neither friction nor nonlinear effects seemed to account for the western boundary current width in the laboratory model, and since the dynamics of the Bering Sea circulation are likely to be linear at first order, we have chosen the simplest model which illustrates the essential point, the existence of the western boundary current.

Consider the steady flow of a homogeneous ocean along a straight (northern) coast located at $x = 0$. The coordinate system is such that x is positive offshelf and y is alongshelf. The depth $h(x)$ is a function of offshelf distance only, and for simplicity bottom friction is pa-

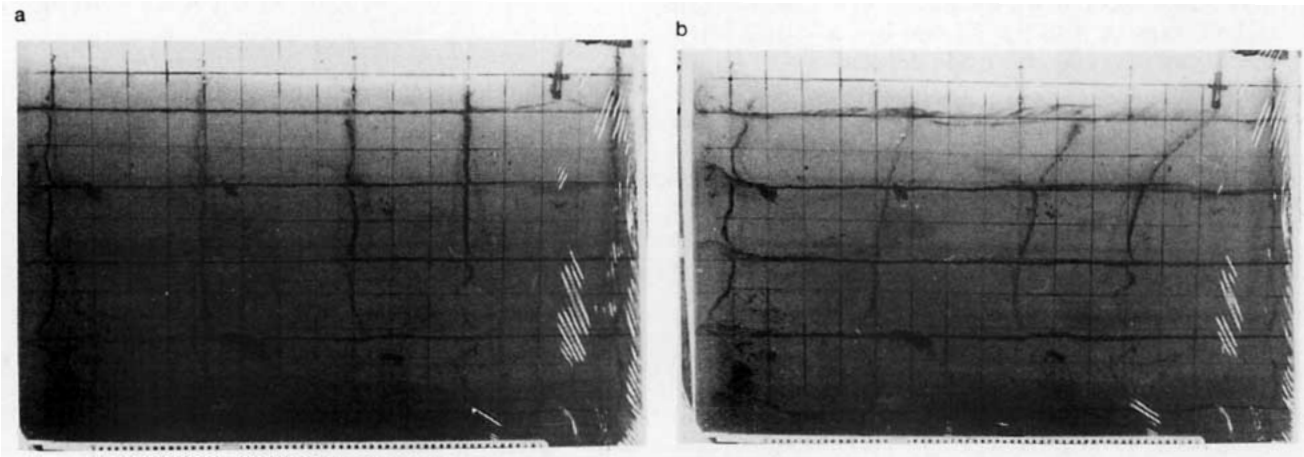

FIG. 9. The same type of experiment as in Figs. 7 and 8 except the sink is near the east coast. The currents are the same as those in the previous figures. Times after start of the sink are 5 and 25 seconds. Period of rotation is 15.4 s and volume flux is 53 $cm^3 s^{-1}$.

rameterized by a constant linear friction coefficient r. The linear depth-averaged equations of motion are:

$$-fv = -g\zeta_x - \frac{ru}{h}, \tag{4.1a}$$

$$fu = -g\zeta_y - \frac{rv}{h}, \tag{4.1b}$$

$$(uh)_x + (vh)_y = 0, \tag{4.1c}$$

where (u, v) are velocities in the (x, y) directions, ζ is sea surface elevation, f the Coriolis parameter, and g gravitational acceleration. Subscripts x, y denote partial differentiation.

A transport streamfunction is defined by

$$uh = -\psi_y, \quad vh = \psi_x \tag{4.2}$$

which satisfies (4.1c). Equations (4.1a, b) and (4.2) combine to form an equation for the streamfunction:

$$\psi_{xx} + \psi_{yy} + \frac{fh_x}{r}\psi_y - \frac{2h_x}{h}\psi_x = 0. \tag{4.3}$$

This is a standard advection–diffusion equation which may be solved (for specified h and appropriate boundary conditions) using the upwind differencing method (nonflux form) of Fiadeiro and Veronis (1977). Situations representative of the laboratory experiment and of the Bering Sea are described next.

a. *Simulation of laboratory experiment*

The model domain for the laboratory experiment is shown in Fig. 10a. Solid cross-shelf walls are placed at $y = 0$ and at $y = 190$ cm. The depth increases linearly with offshore distance, $h = 0.2x$, until it reaches a solid wall at $x = 100$ cm. The outflow at the northern coast occurs through a 5 cm gap located at $x = 0$, 80 cm $< y <$ 85 cm. To simulate the return flow hole (Fig. 6), the inflow at the offshelf (southern) wall occurs through a 5 cm gap located at $x = 100$ cm, $0 < y < 5$ cm. Boundary streamfunctions are specified as $\psi = 1$ on the right of both gaps ($x = 0$, $y > 85$ cm; $0 < x < 100$ cm, $y = 190$ cm; $x = 100$ cm, $y > 5$ cm) and $\psi = 0$ on the left of both gaps ($x = 0$, $y < 80$ cm; $0 < x < 100$ cm, $y = 0$). These values satisfy the boundary condition of no flow through the solid walls, and they impose a unit flow through the domain which can be scaled to any desired total flow. The Coriolis parameter is $f = 4\pi/T = 0.8378$ s^{-1}. Bottom friction is estimated as $r = (\frac{1}{2}\nu f)^{1/2} = 0.065$ cm s^{-1} where $\nu = 0.01$ cm^2 s^{-1} is the kinematic viscosity of water.

The transport streamlines, computed on a 39×21 grid with $\Delta x = \Delta y = 5$ cm, are shown in Fig. 10b. As in the laboratory experiment, the cross-isobath flow occurs almost entirely in a narrow boundary current along the (western) wall at $y = 0$. This current is analogous to the western boundary current described by Stommel (1948) and, as in section 3, has a scale given by $r/fh_x = 0.39$ cm, so the numerical model has not resolved the details of the boundary current, but this does not affect its existence or location. The laboratory experiment (section 4) appeared to develop a much wider boundary current (~8–15 cm).

Upon approaching the northern coast, the boundary current turns to the right and spreads out into an alongshelf boundary layer analogous to the "arrested topographic wave" solution of Csanady (1978). Here the alongshelf flow is nearly geostrophic with bottom friction dominating the nearshore region. This flow is similar to the flow implied by the dye lines in Figs. 7–9.

One might argue that the location of the gap in the offshelf wall could be largely responsible for the cross-isobath flow occurring in a western boundary current. To show that this is not the case, the above numerical simulation was repeated with the offshelf wall removed and a flat-bottom region assumed for $x > 100$ cm ($\psi_{xx} = 0$ at the offshore boundary). The resulting transport streamlines are shown in Fig. 10c. The inflow is now spread over the entire offshelf boundary. However, the inflow turns sharply toward the western boundry ($y = 0$) and flows northward in a pattern almost identical to that in Fig. 10b. Thus, the offshelf boundary has little effect on the interior flow.

b. *Bering Sea simulation*

The barotropic numerical model described above may be used to investigate the dynamics of the mean circulation in the Bering Sea, here represented by the idealized domain shown in Fig. 11a (cf. Fig. 1). The sidewalls represent the Siberian coast ($y = 0$) and the Alaska Peninsula ($y = 1000$ km). The Bering Strait is modeled as an 80 km gap in the northern coast starting at $y = 180$ km. The bottom topography is

$$h(x) = \begin{cases} 40.0 + 4 \times 10^{-4}x, & x < 4 \times 10^5 \text{ m} \\ 200.0 + 0.035(x - 4 \times 10^5), & \\ \qquad 4 \times 10^5 \text{ m} < x < 4.8 \times 10^5 \text{ m} \\ 3000, \quad x > 4.8 \times 10^5 \text{ m}. \end{cases}$$

The depth is 40 m at the northern coast ($x = 0$). The shelf region is modeled with a constant slope of 4×10^{-4}. At 200 m depth ($x = 400$ km) the bottom slope changes to 0.035 to represent the continental slope. The deep Bering Sea is assumed flat at 3000 m depth extending from $x = 480$ km to $x = 540$ km.

An outflow of 1 Sv is assumed uniformly distributed across the Bering Strait. Thus the Alaskan boundary has $\psi = 1$ while the Siberian boundary has $\psi = 0$. At the offshore boundary, the smoothness condition $\psi_{xx} = 0$ is imposed. For lack of a better estimate, the bottom friction coefficient is assumed to be $r = 0.1$ cm s^{-1} which is appropriate for other shelf regions. The Coriolis parameter is $f = 1.27 \times 10^{-4}$ s^{-1}.

The validity of using constant f for a simulation of

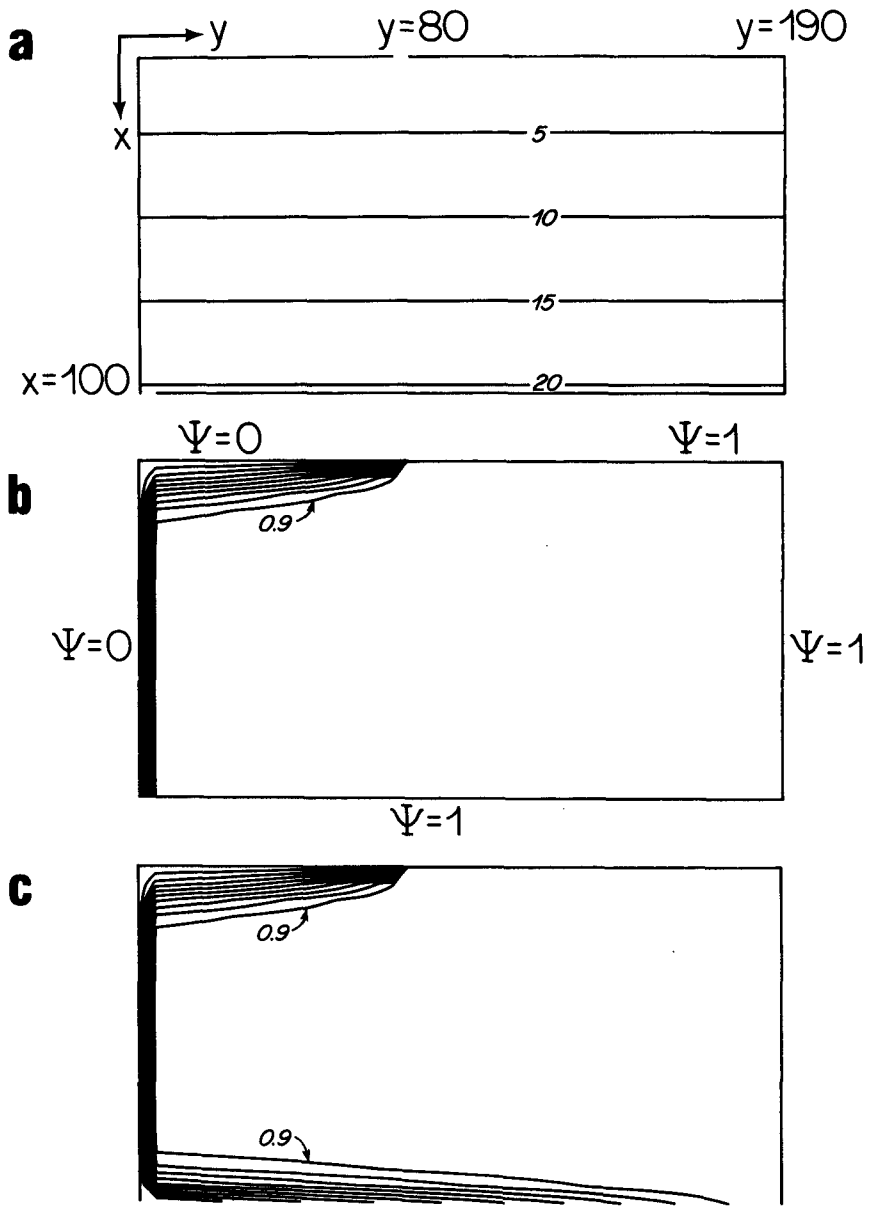

FIG. 10. Numerical simulation of the laboratory experiment (cf Fig. 7). (a) Topography, all lengths in cm. (b) Transport streamlines for the case with the source in the lower left corner. (c) Transport streamlines for the case with no offshelf wall at $x = 100$ cm; ψ is nondimensional, contour interval is 0.1.

the Bering Sea shelf may be checked by estimating planetary β (= the meridional gradient of f) and topographic β, $\beta_T(=fh_x/h)$. For the Bering Sea shelf, $\beta \sim 1 \times 10^{-13}$ cm^{-1} s^{-1} and β_T(at midshelf) $\sim 5 \times 10^{-12}$ cm^{-1} s^{-1}. Thus, the topographic change is dominant by at least one order, and β may be ignored relative to β_T.

The transport streamlines, computed on a 51×28 grid with $\Delta x = \Delta y = 20$ km, are shown in Fig. 11b. Not surprisingly, the model predicts a strong western boundary current similar to the numerical simulation of the laboratory experiment. The inflow is distributed over the entire deep basin but turns sharply toward the Siberian coast where it enters the boundary current. The Stommel scale of the boundary current is proportional to r/fh_x which equals 0.22 km over the slope and 20 km over the shelf. Very little transport occurs over the entire shelf/slope region outside the boundary current.

The predicted velocity structure across the boundary current is shown in Fig. 12 for several offshore positions. The current is about 10–20 cm s^{-1} near the Si-

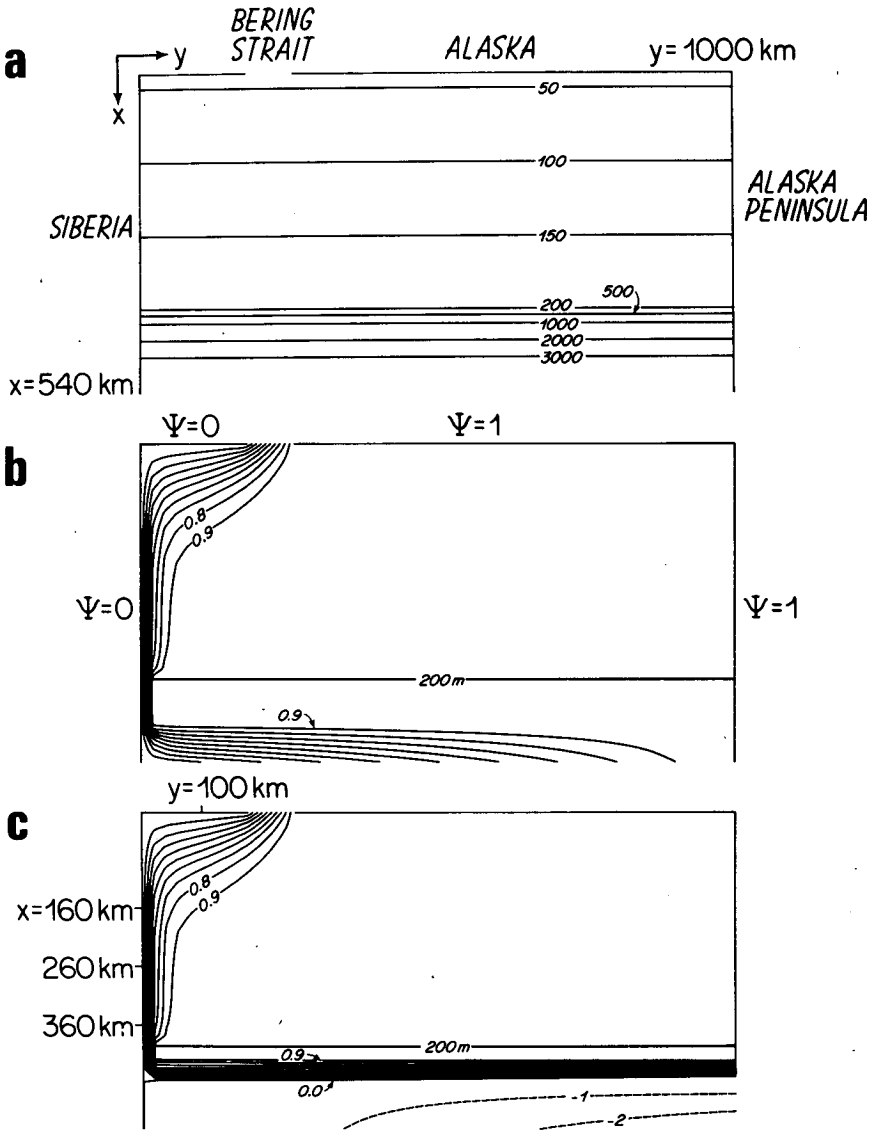

FIG. 11. Numerical simulation of the Bering Sea mean circulation. (a) Simplified topography, depths in m. (b) Transport streamlines for the case with no deep mean inflow imposed at the eastern boundary. (c) Transport streamlines for the case with deep mean inflow imposed at the eastern boundary. ψ has been scaled by the mean flow through the Bering Strait, contour interval 0.1.

berian coast, increasing slightly in the downstream (northward) direction due primarily to the decrease in bottom depth. Figure 13 is a plot of the momentum balance across the boundary current at $x = 260$ km. The along-current flow ($-u$) is geostrophically balanced with the cross-current sea surface slope (ζ_y), and the along-current pressure gradient ($-\zeta_x$) nearly balances the drag due to bottom friction ($-ru/h$).

As the flow approaches the northern boundary, it moves toward the Bering Strait. The momentum balances at $y = 100$ km are shown in Fig. 14. Now the along-shelf current (v) is nearly geostrophically balanced with the offshore sea surface slope (ζ_x). Bottom friction effects are large near the boundary ($x \rightarrow 0$), but they diminish with offshore distance leaving a geostrophic onshore flow. These features are typical of the arrested topographic wave solutions of Csanady (1978).

Observations (section 3) suggest that there may be a substantial mean flow in the deep part of the Bering Sea (~4–5 Sv; Kinder et al., 1975). The effect of this flow may be modeled qualitatively by imposing an inflow transport at the eastern model boundary (Alaska Peninsula) which is uniformly distributed seaward of the 1000 m isobath. The resulting transport streamlines are shown in Fig. 11c. The deep inflow fills the deep basin *and* supplies the transport for the Bering Strait

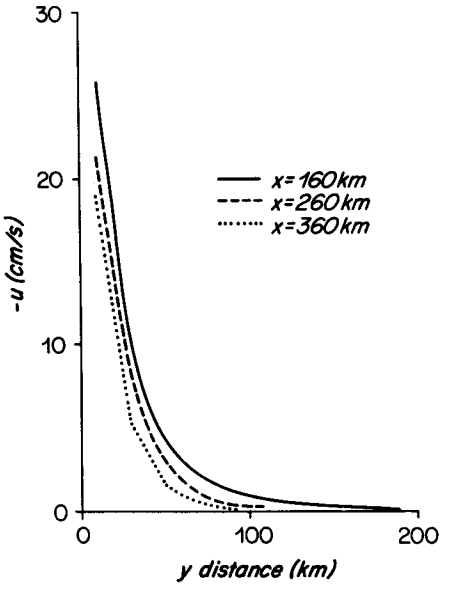

FIG. 12. Numerically predicted velocity structure across the western boundary current at various x locations.

outflow. In effect, a current parallel to the shelf break is generated and held there by the deep flow. This suggests that the Bering Strait outflow may draw most of its water from along the entire slope and little from the deep basin. The deep mean flow is important, however, in that it holds the slope current in place. At the same time the shelf flow is virtually unaltered by the deep mean flow.

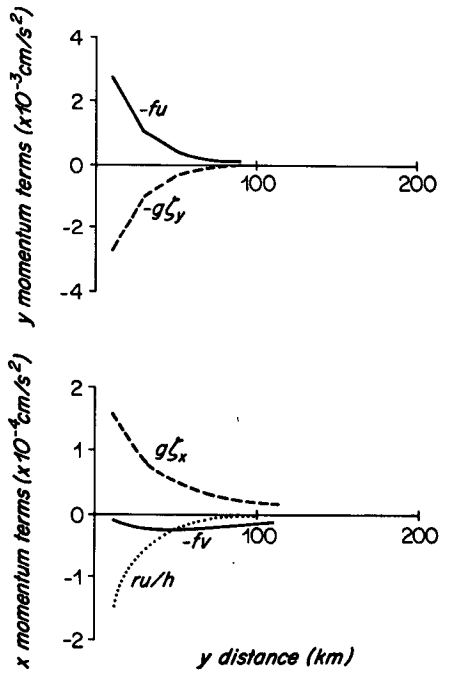

FIG. 13. Numerically predicted momentum balances across the western boundary current at x = 260 km.

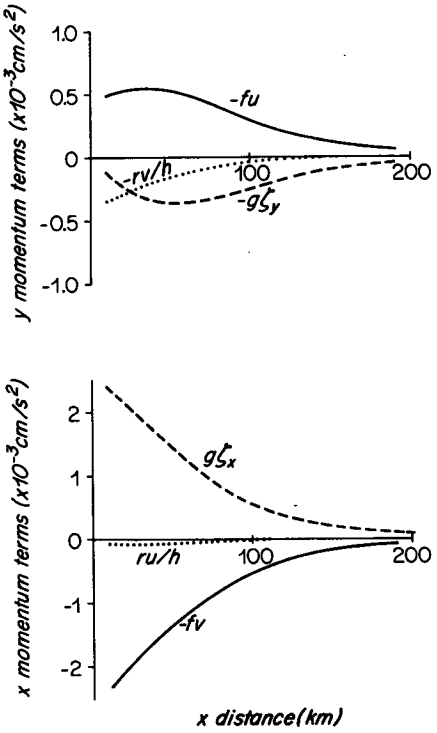

FIG. 14. Numerically predicted momentum balances offshelf (x direction) from the northern boundary at y = 100 km.

6. Discussion

We have argued, based on cumulative observational evidence, that a major part of supply to the mean Bering Strait outflow occurs as a western boundary current. Rather than simulate realistically the eastern Bering Sea shelf circulation, we have attempted to explain the basic dynamics of this current. Since the existence of the current itself is not yet confirmed by direct measurement, our results can be interpreted as a detailed hypothesis.

The laboratory numerical models demonstrated the physical mechanism (the well-known topographic β effect) that may explain this westward intensification. Only the critical features of the shelf were included: shoaling bottom topography, earth's rotation, friction, and a forced outflow. The laboratory model showed that the envisaged mechanism is physically real for the case of a sink located at the coast, and the numerical model showed that this mechanism may be applicable to the Bering Sea. By analogy to Stommel's (1948) explanation of westward intensification in the general oceanic wind-driven circulation, the meridional gradient of the Coriolis parameter is replaced by the gradient of depth, which establishes the sense of direction. The intensification is on the left when facing upslope,

coincidentally on the geographic west side of the Bering Shelf. The numerical model predicts a current width of ~50 km which is directly proportional to the friction parameter, and typical speeds of 10–20 cm s^{-1} which are directly proportional to the imposed transport and inversely proportional to the current width. Thus, while both these estimates agree reasonably with available observations, direct current observations along the Siberian coast are needed to confirm the existence of the current and to compare its structure with the simple model.

There are many aspects of the Bering shelf circulation system that were deliberately excluded from the modeling in order to isolate and clarify the physical mechanism of westward intensification. We discuss briefly some of these omissions, but we feel that our conclusions will not be altered qualitatively when more comprehensive analyses are performed.

Density variations, both vertical and horizontal, are perhaps the most important of the missing effects. Much of the shelf is strongly stratified for at least part of the year (e.g., Ohtani, 1973), and this can partially mitigate the effect of the varying bottom topography. Horizontal density variations are the fundamental cause of the eastern coastal current, and this was absent from both laboratory and numerical models. The Anadyr River discharges into the Gulf of Anadyr, so the dilution of the coastal waters adjacent to Siberia must modify water properties and pressure gradients there as well. Low salinity coastal water does not appear on the western side in the Strait sections of Coachman et al. (1975), although many of these sections stopped short of the Siberian coast. The Siberian runoff may mix completely with the northward flowing Bering Sea/Anadyr water, or it may flow northward or southward as a nearshore coastal current.

Wind stress and the gradients of both wind stress and atmospheric pressure have relatively high values over the Bering Sea, and they demonstrate large fluctuations on scales from days to years (Overland, 1981; Aagaard et al., 1985). While the effect of atmospheric forcing appears small on the southeastern shelf (Schumacher and Kinder, 1983), it dominates the variability near the Strait (Aagaard et al., 1985). Neither the mean atmospheric forcing nor its temporal variation are included in the models.

Tides dominate the kinetic energy over the southeastern shelf (Schumacher and Kinder, 1983), but they are much less important over the northern shelf (Coachman, 1986). The linear friction parameter used in the numerical model was assumed constant, but it would be more accurate to make this a function of the tidal currents which vary across the shelf.

Finally, the actual coasts and bottom topography of the Bering Sea also influence the flow. The Gulf of Anadyr and St. Lawrence Island probably induce curvature and perhaps splitting of the actual northward current. The Siberian Coast is not a vertical wall, and the inshore isobaths parallel the coastline while, in the models, the isobaths were normal to the coast. This may move the physical current away from the coast and cause it to spread laterally.

There may exist other oceanographic situations where the topographic beta mechanism is important in a similar manner, i.e. fluid is forced across shoaling bathymetry on scales where the Coriolis effect is significant. One such place may be the western Mediterranean where the outflowing Mediterranean Water is apparently forced across shoaling topography towards the Strait of Gibraltar. This flow forms a narrow boundary current against the African slope (i.e., left-hand side looking upslope; the zonal bathymetric gradient is relevant since the flow is forced to the west; Parrilla et al., 1986; Whitehead, 1985).

Acknowledgments. The authors thank Robert E. Frazel who assisted with and photographed the laboratory experiments, and David Musgrave who reviewed an early version of the manuscript. Several discussions with Joe Pedlosky provided valuable insight concerning the laboratory western boundary current. Anonymous reviewers also gave helpful criticisms. T.H.K was supported by the Coastal Sciences Division of the Office of Naval Research. D.C.C was supported by National Science Foundation Grant OCE84-17769. JAW was supported by Office of Naval Research Contract N00014-85-C-0001, NR083-004.

REFERENCES

Aagaard, K., A. T. Roach and J. D. Schumacher, 1985: On the wind-driven variability of the flow through Bering Strait. *J. Geophys. Res.*, **90**, 7213–7221.

Baker, D. J., Jr., and A. R. Robinson, 1969: A laboratory model for the general oceanic circulation. *Phil. Trans. Roy. Soc. London*, **A265**, 533–566.

Beardsley, R. C., 1969: A laboratory model of the wind-driven circulation. *J. Fluid Mech.*, **38**, 255–272.

Coachman, L. K., 1986: Circulation, water masses, and fluxes on the southeastern Bering Sea shelf. *Contin. Shelf Res.*, **5**, 23–108.

——, and K. Aagaard, 1981: Reevaluation of water transports in the vicinity of Bering Strait. *The Eastern Bering Sea Shelf: Oceanography and Resources*, D. W. Hood and H. A. Calder, Eds., University of Washington Press, pp. 95–110.

——, —— and R. B. Tripp, 1975: *Bering Strait: The Regional Physical Oceanography.* University of Washington Press, 172 pp.

Csanady, G. T., 1978: The arrested topographic wave. *J. Phys. Oceanogr.*, **8**, 47–62.

Fiadeiro, M. E., and G. Veronis, 1977: On weighted-mean schemes for the finite-difference approximation to the advection-diffusion equation. *Tellus*, **29**, 512–522.

Hughes, F. W., L. K. Coachman and K. Aagaard, 1974: Circulation, transport, and water exchange in the western Bering Sea. *Oceanography and Bering Sea with Emphasis on Renewable Resources*, D. W. Hood and E. J. Kelley, Eds., University of Alaska, pp. 59–98.

Ingraham, W. H., Jr., 1981: Shelf environment. *The Eastern Bering Sea Shelf: Oceanography and Resources*, D. W. Hood and J. A. Calder, Eds., University of Washington Press, pp. 455–469.

Kinder, T. H., and J. D. Schumacher, 1981a: Hydrographic structure over the continental shelf of the southeastern Bering Sea. *The Eastern Bering Sea Shelf: Oceanography and Resources*, D. W.

Hood and J. A. Calder, Eds., University of Washington Press, pp. 31–52.

——, and ——, 1981b: Circulation over the continental shelf of the southeastern Bering Sea. *The Eastern Bering Sea Shelf: Oceanography and Resources,* D. W. Hood and J. A. Calder, Eds., University of Washington Press, pp. 53–75.

——, L. K. Coachman and J. A. Galt, 1975: The Bering slope current system. *J. Phys. Oceanogr.*, **5,** 231–244.

——, J. D. Schumacher and D. V. Hansen, 1980: Observation of a baroclinic eddy: An example of mesoscale variability in the Bering Sea. *J. Phys. Oceanogr.*, **10,** 1228–1245.

Kuo, H.-H., and G. Veronis, 1971: The source-sink flow in a rotating system and its oceanic analogy. *J. Fluid Mech.*, **45,** 441–466.

Muench, R. D., and J. D. Schumacher, 1985: On the Bering Sea ice edge front. *J. Geophys. Res.*, **90,** 3185–3197.

Munk, W. H., 1950: On the wind-driven ocean circulation. *J. Meteor.*, **7,** 79–93.

Ohtani, K., 1973: Oceanographic structure of the Bering Sea. *Mem. Fac. Fish. Hokkaido Univ.*, **21,** 65–106.

Overland, J. E., 1981: Marine climatology of the Bering Sea. *The Eastern Bering Sea Shelf: Oceanography and Resources,* D. W. Hood and J. A. Calder, Eds., University of Washington Press, pp. 15–27.

Paluskiewicz, T., and H. J. Niebauer, 1984: Satellite observations of circulation in the eastern Bering Sea. *J. Geophys. Res.*, **89,** 3663–3678.

Parrilla, G., T. H. Kinder and R. H. Preller, 1986: Deep and intermediate Mediterranean water in the western Alboran Sea. *Deep-Sea Res.*, **33,** 55–88.

Pedlosky, J., 1979: *Geophysical Fluid Dynamics,* Springer-Verlag, 624 pp.

Roden, G. I., 1967: On river discharge into the northeastern Pacific Ocean and Bering Sea. *J. Geophys. Res.*, **72,** 5613–5629.

Royer, T. C., and W. J. Emery, 1984: Circulation in the Bering Sea 1982–83, based on satellite tracked drifter observations. *J. Phys. Oceanogr.*, **14,** 1914–1920.

Sambrotto, R. N., J. J. Goering and C. P. McRoy, 1984: Large yearly production of phytoplankton in the western Bering Strait. *Science,* **225,** 1147–1150.

Schumacher, J. D., and T. H. Kinder, 1983: Low-frequency current regimes over the Bering Sea shelf. *J. Phys. Oceanogr.*, **13,** 607–623.

——, K. Aagaard, C. H. Pease and R. B. Tripp, 1983: Effects of a shelf polyna on flow and water properties in the northern Bering Sea. *J. Geophys. Res.*, **88,** 2723–2732.

Springer, A. M., and D. G. Roseneau, 1985: Copepod-based food webs: Auklets and oceanography in the Bering Sea. *Mar. Ecol. Prog. Ser.*, **21,** 229–237.

Stigebrandt, A., 1984: The North Pacific: A global scale estuary. *J. Phys. Oceanogr.*, **14,** 464–470.

Stommel, H., 1948: The westward intensification of wind-driven ocean circulation. *Trans. Amer. Geophys. Union,* **29,** 202–206.

——, A. B. Arons and A. J. Faller, 1958: Some examples of stationary planetary flow patterns in bounded basins. *Tellus,* **10,** 179–187.

Takenouti, A. Y., and K. Ohtani, 1974: Currents and water masses in the Bering Sea: A review of Japanese work. *Oceanography of the Bering Sea with an Emphasis on Renewable Resources,* D. W. Hood and E. J. Kelley, Eds., University of Alaska, pp. 39–57.

Whitehead, J. A. Jr., 1985: A laboratory study of gyres and uplift near the Strait of Gibraltar. *J. Geophys. Res.*, **90,** 7045–7060. (Also correction, *J. Geophys. Res.*, **90,** 12011–12013.)